Fermi-level pinning and intrinsic surface states of $Al_{1-x}In_xN(10\bar{1}0)$ surfaces

V. Portz,[1] M. Schnedler,[1] L. Lymperakis,[2] J. Neugebauer,[2] H. Eisele,[3] J.-F. Carlin,[4] R. Butté,[4] N. Grandjean,[4] R. E. Dunin-Borkowski,[1] and Ph. Ebert[1,a)]
[1]*Peter Grünberg Institut, Forschungszentrum Jülich GmbH, 52425 Jülich, Germany*
[2]*Computational Materials Department, Max-Plank-Institut für Eisenforschung GmbH, Max-Plank-Str. 1, 40237 Düsseldorf, Germany*
[3]*Technische Universität Berlin, Institut für Festkörperphysik, Hardenbergstr. 36, 10623 Berlin, Germany*
[4]*Institute of Physics, Ecole Polytechnique Fédérale de Lausanne, 1015 Lausanne, Switzerland*

(Received 6 October 2016; accepted 21 December 2016; published online 10 January 2017)

The electronic structure of $Al_{1-x}In_xN(10\bar{1}0)$ surfaces is investigated by cross-sectional scanning tunneling spectroscopy and density functional theory calculations. The surface exhibits empty Al and/or In-derived dangling bond states, which are calculated to be within the fundamental bulk band gap for In compositions smaller than 60%. The energy of the lowest empty In-derived surface state is extracted from the tunnel spectra for lattice-matched $Al_{1-x}In_xN$ with In compositions of $x = 0.19$ and $x = 0.20$ to be $E_C - 1.82 \pm 0.41$ and $E_C - 1.80 \pm 0.56$ eV, respectively, in good agreement with the calculated energies. Under growth conditions, the Fermi level is hence pinned (unpinned) for In compositions smaller (larger) than 60%. The analysis of the tunnel spectra suggests an electron affinity of ~3.5 eV for nonpolar lattice-matched $Al_{1-x}In_xN$ cleavage surfaces, which is large compared to linearly interpolated values of polar AlN and InN (0001) surfaces. *Published by AIP Publishing.* [http://dx.doi.org/10.1063/1.4973765]

Group III-nitride semiconductors have excellent optoelectronic properties from the ultraviolet to the red spectral range. Within the different group III-nitride semiconductors, $Al_{1-x}In_xN$ attracted significant attention over the past decade, since on the one hand, it exhibits a substantially different refractive index and band gap as compared to GaN, and on the other hand, it can be grown lattice-matched to GaN for an In content of about 19%.[1,2] Hence, $Al_{1-x}In_xN$ is a promising material for applications in optoelectronics as well as in high electron mobility transistors.[3–7]

Thus far mostly polar *c*-plane grown $Al_{1-x}In_xN$ layers were investigated, but recently growth along the nonpolar directions has attracted significant interest[8–11] due to the absence of electric fields caused by piezoelectricity and spontaneous polarization mismatch.[12] It is known that the presence of surface states and the Fermi level position at the growth surface critically affect atomic processes during growth, such as the incorporation of dopants and impurities.[13,14] However, current knowledge about the electronic structure of nonpolar surfaces is limited to GaN and InN only.[15–19] Hence, the lack of knowledge of the electronic structure of $Al_{1-x}In_xN$ nonpolar surfaces is detrimental for achieving controlled growth conditions along nonpolar directions.

Here, we study the electronic structure of $Al_{1-x}In_xN$ $(10\bar{1}0)$ cleavage surfaces by cross-sectional scanning tunneling microscopy (STM) and spectroscopy (STS) combined with density functional theory (DFT) calculations. We calculated that $Al_{1-x}In_xN$ has empty surface states within the fundamental band gap for In compositions $x \lesssim 0.6$. The lowest energy empty surface state arises from the In dangling bond state. Its energy is derived experimentally from the tunnel spectra acquired on $Al_{0.81}In_{0.19}N$ and $Al_{0.80}In_{0.20}N(10\bar{1}0)$ cleavage surfaces to be ~1.8 eV below the conduction band edge, in good agreement with the theory. In addition, we identified a bias polarity-dependent Fermi-level pinning.

We investigated two different $Al_{1-x}In_xN$/GaN heterostructures grown by metal organic vapor phase epitaxy on *c*-plane free-standing GaN pseudosubstrates. Heterostructure 1 (H1) is a distributed Bragg reflector (DBR), consisting of 42 undoped pairs of 48.6 nm $Al_{0.80}In_{0.20}N$ followed by 36.5 nm GaN, deposited on a 1 μm thick 3×10^{18} cm^{-3} *n*-doped GaN buffer layer. The In content x is slightly reduced at the $Al_{0.80}In_{0.20}N$/GaN interface. Heterostructure 2 (H2) contains five 31 nm thick $Al_{0.81}In_{0.19}N$ layers separated by 105 nm thick *n*-type GaN interlayers, deposited on a 500 nm thick *n*-doped GaN buffer layer and capped by a 1 μm thick *n*-type GaN layer. Each $Al_{1-x}In_xN$ layer is unintentionally *n*-doped. The layer thicknesses and the In content of 20 ± 0.5% (H1) and 19 ± 0.5% (H2) were determined by high resolution X-ray diffraction. At this In content, the $Al_{1-x}In_xN$ layers are almost lattice matched to GaN along the *a* direction.[20] The $Al_{1-x}In_xN$ layer thickness is below the critical thickness for the development of V-defects.[21]

All samples were cut from the heterostructures, contacted by a sputtered Au layer, and cleaved in ultrahigh vacuum ($p < 10^{-8}$ Pa) to obtain clean $(10\bar{1}0)$ surfaces. The cleavage surfaces are investigated by cross-sectional STM and STS without interruption of the vacuum. A cross-sectional view of H1 is shown in Fig. 1 in which from left to right, the GaN buffer layer and the first six $Al_{0.80}In_{0.20}N$/GaN pairs of the DBR can be identified. The $Al_{0.80}In_{0.20}N$ layers appear brighter than the surrounding GaN.

We measured the scanning tunneling spectra on various cleavage surfaces of the $Al_{1-x}In_xN$ layers in H1 and H2. The black dots in Fig. 2 show an example of an $I(V)$ tunnel spectrum that was measured on H2. The spectra show a typical semiconducting behavior, with a tunnel current at positive

a)Electronic mail: p.ebert@fz-juelich.de

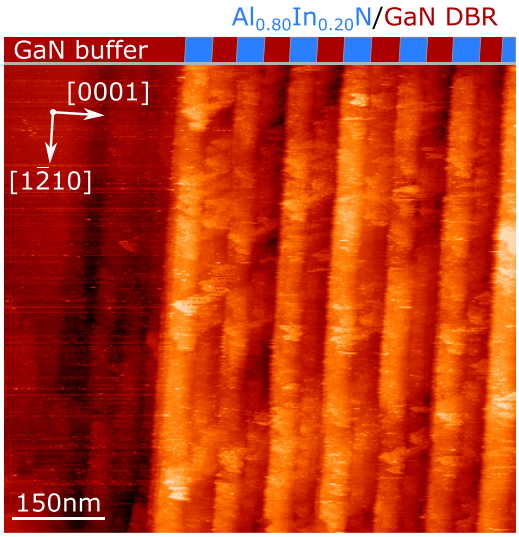

FIG. 1. Cross-sectional STM overview image of the (10$\bar{1}$0) cleavage surface through the $Al_{0.80}In_{0.20}N$/GaN distributed Bragg reflector heterostructure (H1) measured at +3.8 V and 100 pA. In the STM image, the $Al_{0.80}In_{0.20}N$ layers appear brighter than the surrounding GaN. On the left hand side, part of the GaN buffer is visible.

and negative voltages, separated by an asymmetric ~3 V wide voltage range, where no tunnel current is detected. This is the signature of the band gap of the semiconductor.[22] The onset voltages of the tunnel current are at +2 V and −1 V, respectively.

In order to interpret the measured tunnel spectra, we performed simulations of the tunnel current with a 3D finite difference calculation. The electrostatic potential is computed for a tip-vacuum-semiconductor system by solving the Poisson equation and additionally the continuity equations for electrons and holes following the methodology in Refs. 23 and 24. The simulated tunnel currents are shown in Fig. 2 as lines for both unpinned and pinned $Al_{1-x}In_xN(10\bar{1}0)$ surfaces.

The unpinned case, where no surface state is included in the calculation, is represented by the red solid and dashed

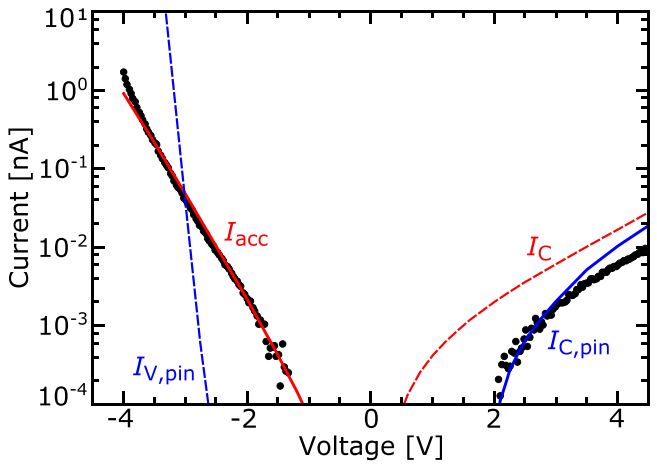

FIG. 2. Scanning tunneling spectrum measured on the $Al_{0.81}In_{0.19}N(10\bar{1}0)$ surface. The experimental data is represented by the black dots measured at a tip-sample separation fixed by a set voltage of −3.6 V and a set current of 150 pA. The lines illustrate calculations of the tunnel current assuming no intrinsic surface state within the band gap (red) and an empty surface state at $E_C - 1.8$ eV, which pins the Fermi energy (blue). All simulations are performed for the same tip-sample separation.

lines. Without pinning, the electric field between tip and semiconductor penetrates into the semiconductor and induces a band bending. At negative voltages, the tip-induced downward band bending drags the conduction band edge E_C below the Fermi energy (E_F), inducing an electron accumulation in the conduction band. The electrons in this accumulation zone can tunnel into the tip at negative voltages corresponding to energies within the band gap. Hence, a tunnel current flows at small negative voltages already. This calculated accumulation tunnel current (I_{acc}) fits well to the measured data. Note, the tip-sample separation was used as fit parameter to adjust the tunnel current at negative voltages. At positive voltages, electrons are expected to tunnel into the empty conduction band. However, the calculation without pinning yields a too high tunnel current I_C and an onset voltage too close to zero. Hence, it does not describe the measured onset around +2 V.

For calculating the pinned case, we added an intrinsic empty surface state 1.8 eV below the conduction band edge with a FWHM of 0.2 eV and a concentration of 7×10^{13} cm^{-2}. This concentration value corresponds to the concentration of In atoms in the surface layer, where the dangling bond state is localized (see below). For the calculation of the pinned surface, the same tip-sample separation is used as for the unpinned surface. The simulated tunnel spectra of the pinned surface are illustrated by the blue solid and dashed lines in Fig. 2. The pinning removes the tip-induced band bending and thus at negative voltages, no accumulation of electrons in the conduction band occurs. Thus the current is solely given by tunneling from the valence band into the tip ($I_{V,pin}$), which is however too small. At positive voltages, the midgap pinning shifts the onset of electrons tunneling from the tip into the conduction band ($I_{C,pin}$) to higher voltages. This model provides a good description of the tunnel current at positive voltages for a surface state 1.8 eV below the conduction band edge. Thus, the best fit is obtained for an unpinned surface at negative voltages (solid red line in Fig. 2) and a surface pinned by a surface state at positive voltages (solid blue line in Fig. 2). This suggests a polarity-dependent pinning by the empty intrinsic surface state, in analogy to GaN(10$\bar{1}$0) surfaces.[19]

In order to identify the origin of the midgap surface state, we have performed first principles calculations within DFT using the local density approximation (LDA) and the projector augmented wave approach (PAW).[25,26] In a first step, the *c*-lattice constant (along ⟨0001⟩) has been optimized for a 32 atom bulk supercell, which is biaxially strained in the basal plane to GaN and where the group-III sublattice is occupied with 3 In (and 13 Al) atoms, reflecting the In composition. Then the *m*-plane surfaces are modeled using slabs of 16-monolayers (MLs) AlN with the aforementioned lattice constant. A plane-wave energy cutoff of 450 eV was used and the position of the atoms in the 8 topmost monolayers (MLs) was fully relaxed. The In semicore *d* states are treated explicitly as valence electrons, and the triply coordinated lowermost Al and N atoms were passivated with pseudohydrogen atoms of partial charge 1.25 and 0.75, respectively. In the top layer, one Al is replaced by an In atom. By modifying the lateral size of the supercell (i.e., $n \times m$, n and m denote the repetition along ⟨11$\bar{2}$0⟩ and ⟨0001⟩, respectively)

the surface In composition is effectively changed within the whole range between pure AlN and pure InN.

Figures 3(a) and 3(b) show the calculated band structure and density of states (DOS), respectively, for the example of a 2×3 surface unit cell with one In atom replacing a surface Al atom (corresponding to an In composition of 16.7% in the surface layer). In the band structure, various states can be identified: Within the band gap, a band of states (labeled S_N) occurs at energies between 0 and 0.5 eV. The charge density of these states shown in Fig. 3(e) reveals that this band of states corresponds to the filled nitrogen dangling bonds with *p* orbital character. The next state in the band gap (S_{In}) 2.4 eV above E_V corresponds to the empty dangling bond above the In atom as visible in Fig. 3(d). Finally, several surface states appear near the conduction band edge (labeled S_{Al}). Figure 3(c) shows the charge density of the highest one. These states correspond to the empty Al dangling bonds. Both, the empty In and Al dangling bond states have a mixed *s* and *p* orbital character.

Figure 4 (blue dots) illustrates the calculated energy minima of the lowermost empty In/Al-derived surface state S_{In} as a function of the In composition *x* of $Al_{1-x}In_xN$. The energies of the surface state minima are given relative to the valence band edge of pure AlN. The valence and conduction band edges shown as black and gray curves, respectively, were derived using composition-dependent bowing parameters calculated using a tight-binding (TB) model for the compositions marked by crosses.[27] The blue symbols illustrate that the lowermost empty dangling bond is within the fundamental band gap for In compositions $x \lesssim 0.6$. For pure InN, the empty surface state is within the conduction band in

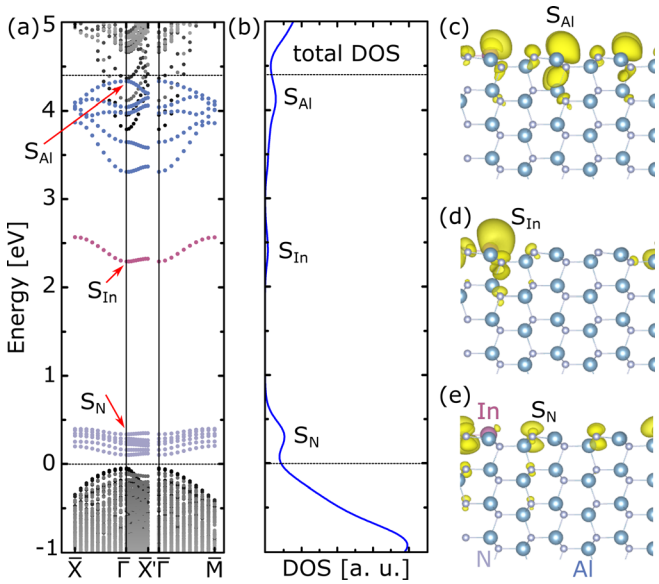

FIG. 3. (a) Band structure of the $Al_{0.83}In_{0.17}N(10\bar{1}0)$ surface. S_N denotes the occupied N-derived surface states, S_{In} the In-derived unoccupied surface state, and S_{Al} the unoccupied Al-derived surface states. Gray dots denote the projected bulk band structure of AlN at the lattice constant of $Al_{0.83}In_{0.17}N$. The upper and lower horizontal lines at 4.4 eV and 0 eV mark the bulk CBM and VBM of AlN at its optimum lattice constant, respectively. The absolute position of the corresponding band structures has been obtained by aligning the bulk ionization potentials to the vacuum level. (b) Total density of states (DOS). (c), (d), (e) show the charge density of the S_{Al}, S_{In}, and S_N states, respectively. Al, In, and N atoms are shown as medium-sized blue, large-sized purple, and small gray dots, respectively.

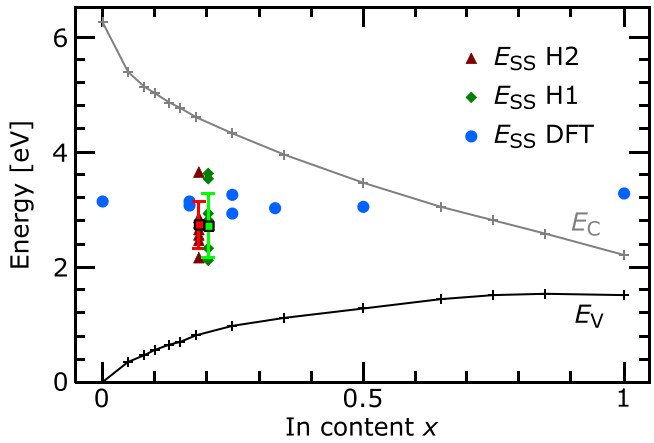

FIG. 4. Energy position of the lowest empty cation derived surface state on $Al_{1-x}In_xN(10\bar{1}0)$ surfaces as a function of In composition *x*. The conduction band (E_C, gray) and valence band (E_V, black) edges were calculated using Ref. 27. Blue dots show the calculated energy position of the lowermost empty cation-derived surface state. This state is the In-derived dangling bond (Al-derived surface stares are significantly higher in energy), except for pure AlN where it is the Al-derived dangling bond. The green diamonds and red triangles show the energy of the surface state E_{SS} extracted from scanning tunneling spectra with the help of tunnel current simulations for $Al_{0.80}In_{0.20}N$ and $Al_{0.81}In_{0.19}N$ layers in heterostructure 1 and 2, respectively. The dark framed symbols with error bars show the respective average values.

agreement with previous calculations and experiments.[13,17] For pure AlN, the surface state is located at midgap, consistent with previous calculations.[28]

In order to compare the calculated results with our experiments, we analyzed a large number of spectra acquired on different cleavage surfaces of both heterostructures with different W tips. All spectra exhibit similar onset voltages. In order to extract the energetic position E_{SS} of the lowermost empty surface state, we simulated each spectrum using the energy position E_{SS} and the tip-sample separation as fit parameters. This procedure is done in analogy to that discussed above for the spectrum shown in Fig. 2. The best fit of the onset voltage of the tunnel current at positive voltages is used as a criterion to extract the energy of the lowest midgap surface state. The green diamonds and red triangles show the obtained surface state energy for the $Al_{0.80}In_{0.20}N$ and $Al_{0.81}In_{0.19}N$ layers in H1 and H2, respectively. The range of surface state energies is attributed to variations in the tip states and fluctuations in the composition of the ternary alloy.[29] The respective average values are $E_C - 1.80 \pm 0.56$ eV and $E_C - 1.82 \pm 0.41$ eV. They are shown as dark framed symbols with error bars. The energy values of the surface state are measured *relative to the conduction band edge* E_C. In contrast, the calculated surface state energies are most accurate *relative to the valence band edge* E_V. Thus, if the experimental band gaps are larger than the calculated ones in Fig. 4, the experimental values of the surface state energy shift 1:1 upward relative to the calculated ones. Indeed, there are indications from experiments that the real band gap of $Al_{0.81}In_{0.19}N$ is 4.2 eV,[30] i.e., 0.5 eV larger than the calculated one. Hence, our experimental data points may need to be shifted up to 0.5 eV upward relative to the calculated ones. Independent of this uncertainty, the experimental results agree well with the calculated energy minima of the lowest empty surface state.

At this stage, we address the origin of pinning. Although we frequently observe cleavage steps on the surface, the concentration of step states (assuming one state per lattice constant) is one order of magnitude lower than the surface density of In dangling bonds (S_{In}). Hence, the steps cannot induce an extrinsic pinning. The polarity dependent Fermi level pinning is only due to the intrinsic In surface dangling bond state.

Finally, the simulations of the tunnel spectra require surprisingly large electron affinities. The best fits are obtained for $\chi \approx 3.5\,\text{eV}$. Unfortunately, nothing is known about the composition dependence of the electron affinity. Hence, as a first approximation, we assumed a linear change in the electron affinity between AlN and InN, the latter being assumed to amount to 5.7 eV.[31] This would yield an electron affinity of ~3.0 eV for AlN. This value for a nonpolar stoichiometric AlN cleavage surface is larger than the previously reported electron affinities determined on polar surfaces ranging from 0.6 to 2.16 eV.[32–34] These polar (0001) surfaces were prepared by N sputtering and annealing cycles and the investigated surfaces exhibited a 1×1 reconstruction. Under such conditions, the surfaces can be expected to be non-stoichiometric and covered by one or two Al adlayers which may be partially disordered.[35] These adlayers fill the band gap with surface states[28] and may affect the electron affinity. In contrast, here we investigate the cleaved stoichiometric surfaces without metallic adlayers. This suggests that the electron affinity of group III-nitride semiconductors needs to be reassessed.

In conclusion, we investigated the electronic structure of $Al_{1-x}In_xN(10\bar{1}0)$ surfaces by cross-sectional scanning tunneling spectroscopy and density functional theory calculations. Calculations yield empty Al- and/or In-derived dangling bond states within the band gap for In compositions smaller than 60%. We extracted the energy of the lowest empty In-derived surface state from tunnel spectra acquired on lattice-matched $Al_{1-x}In_xN$ layers with In compositions of $x = 0.19$ and $x = 0.20$ to be $E_C - 1.82 \pm 0.41\,\text{eV}$ and $E_C - 1.80 \pm 0.56\,\text{eV}$, respectively, in good agreement with the calculated energies. Based on these results, we conclude that under growth conditions, the Fermi level is pinned by the In-derived dangling bond state for In compositions smaller than about 60%. For larger In concentrations, no Fermi level pinning is present. Furthermore, the simulation of the tunnel spectra yields the best fits for an electron affinity of ~3.5 eV for nonpolar cleavage surfaces, which is significantly larger than the linearly interpolated values of polar AlN and InN (0001) surfaces.

The authors thank K. H. Graf for technical support and the Deutsche Forschungsgemeinschaft under Grant Nos. Eb 197/5-1 and Ei 788/2-1, the Collaborative Research Center Sfb 787, TP A4, and the Impuls und Vernetzungsfonds of the Helmholtz-Gemeinschaft Deutscher Forschungszentren under Grant No. HIRG-0014 for financial support.

[1]J.-F. Carlin and M. Ilegems, Appl. Phys. Lett. **83**, 668 (2003).
[2]R. Butté, J.-F. Carlin, E. Feltin, M. Gonschorek, S. Nicolay, G. Christmann, D. Simeonov, A. Castiglia, J. Dorsaz, H. J. Buehlmann, S. Christopoulos, G. B. H. von Högersthal, A. J. D. Grundy, M. Mosca, C. Pinquier, M. A. Py, F. Demangeot, J. Frandon, P. G. Lagoudakis, J. J. Baumberg, and N. Grandjean, J. Phys. D: Appl. Phys. **40**, 6328 (2007).
[3]J.-F. Carlin, J. Dorsaz, E. Feltin, R. Butté, N. Grandjean, M. Ilegems, and M. Laügt, Appl. Phys. Lett. **86**, 031107 (2005).
[4]M. Gonschorek, J.-F. Carlin, E. Feltin, M. A. Py, and N. Grandjean, Appl. Phys. Lett. **89**, 062106 (2006).
[5]J. Kotani, A. Yamada, T. Ishiguro, S. Tomabechi, and N. Nakamura, Appl. Phys. Lett. **108**, 152109 (2016).
[6]H. F. Sun, A. R. Alt, H. Benedickter, E. Feltin, J.-F. Carlin, M. Gonschorek, N. Grandjean, and C. R. Bolognesi, IEEE Electron Device Lett. **31**, 957 (2010).
[7]N. Sarazin, E. Morvan, M. A. D. Poisson, M. Oualli, C. Gaquiere, O. Jardel, O. Drisse, M. Tordjiman, M. Magis, and S. L. Delage, IEEE Electron Device Lett. **31**, 11 (2010).
[8]T. Kajima, A. Kobayashi, K. Ueno, K. Shimomoto, T. Fujii, J. Ohta, H. Fujioka, and M. Oshima, Jpn. J. Appl. Phys., Part 1 **49**, 070202 (2010).
[9]M. R. Laskar, T. Ganguli, A. A. Rahman, A. Arora, N. Hatui, M. R. Gokhale, S. Ghosh, and A. Bhattacharya, Appl. Phys. Lett. **98**, 181108 (2011).
[10]C. Durand, C. Bougerol, J.-F. Carlin, G. Rossbach, F. Godel, J. Eymery, P.-H. Jouneau, A. Mukhtarova, R. Butté, and N. Grandjean, ACS Photonics **1**, 38 (2014).
[11]E. R. Buß, P. Horenburg, U. Rossow, H. Bremers, T. Meisch, M. Caliebe, F. Scholz, and A. Hangleiter, Phys. Status Solidi B **253**, 84 (2016).
[12]P. Waltereit, O. Brandt, A. Trampert, H. T. Grahn, J. Menniger, M. Ramsteiner, M. Reiche, and K. H. Ploog, Nature **406**, 865 (2000).
[13]C. G. Van de Walle and D. Segev, J. Appl. Phys. **101**, 081704 (2007).
[14]L. Lymperakis and J. Neugebauer, Phys. Rev. B **79**, 241308 (2009).
[15]L. Ivanova, S. Borisova, H. Eisele, M. Dähne, A. Laubsch, and Ph. Ebert, Appl. Phys. Lett. **93**, 192110 (2008).
[16]M. Bertelli, P. Löptien, M. Wenderoth, A. Rizzi, R. G. Ulbrich, M. C. Righi, A. Ferretti, L. Martin-Samos, C. M. Bertoni, and A. Catellani, Phys. Rev. B **80**, 115324 (2009).
[17]Ph. Ebert, S. Schaafhausen, A. Lenz, A. Sabitova, L. Ivanova, M. Dähne, Y.-L. Hong, S. Gwo, and H. Eisele, Appl. Phys. Lett. **98**, 062103 (2011).
[18]L. Lymperakis, P. H. Weidlich, H. Eisele, M. Schnedler, J.-P. Nys, B. Grandidier, D. Stievenard, R. E. Dunin-Borkowski, J. Neugebauer, and Ph. Ebert, Appl. Phys. Lett. **103**, 152101 (2013).
[19]M. Schnedler, V. Portz, H. Eisele, R. E. Dunin-Borkowski, and Ph. Ebert, Phys. Rev. B **91**, 205309 (2015).
[20]G. Cosendey, J.-F. Carlin, N. A. K. Kaufmann, R. Butté, and N. Grandjean, Appl. Phys. Lett. **98**, 181111 (2011).
[21]G. Perillat-Merceroz, G. Cosendey, J.-F. Carlin, R. Butté, and N. Grandjean, J. Appl. Phys. **113**, 063506 (2013).
[22]R. M. Feenstra and J. A. Stroscio, J. Vac. Sci. Technol. B **5**, 923 (1987).
[23]M. Schnedler, V. Portz, P. H. Weidlich, R. E. Dunin-Borkowski, and Ph. Ebert, Phys. Rev. B **91**, 235305 (2015).
[24]M. Schnedler, R. E. Dunin-Borkowski, and Ph. Ebert, Phys. Rev. B **93**, 195444 (2016).
[25]G. Kresse and J. Furthmüller, Phys. Rev. B **54**, 11169 (1996).
[26]G. Kresse and J. Hafner, Phys. Rev. B **47**, 558 (1993).
[27]S. Schulz, M. A. Caro, L.-T. Tan, P. J. Parbrook, R. W. Martin, and E. P. O'Reilly, Appl. Phys. Express **6**, 121001 (2013).
[28]M. S. Miao, A. Janotti, and C. G. Van de Walle, Phys. Rev. B **80**, 155319 (2009).
[29]V. Portz, M. Schnedler, M. Duchamp, F.-M. Hsiao, H. Eisele, J.-F. Carlin, R. Butté, N. Grandjean, R. E. Dunin-Borkowski, and Ph. Ebert, Appl. Phys. Lett. **109**, 132102 (2016).
[30]E. Sakalauskas, H. Behmenburg, C. Hums, P. Schley, G. Rossbach, C. Giesen, M. Heuken, H. Kalisch, R. H. Jansen, J. Bläsing, A. Dadgar, A. Krost, and R. Goldhahn, J. Phys. D: Appl. Phys. **43**, 365102 (2010).
[31]J. Wu, W. Walukiewicz, S. X. Li, R. Armitage, J. C. Ho, E. R. Weber, E. E. Haller, H. Lu, W. J. Schaff, A. Barcz, and R. Jakiela, Appl. Phys. Lett. **84**, 2805 (2004).
[32]V. M. Bermudez, T. M. Jung, K. Doverspike, and A. E. Wickenden, J. Appl. Phys. **79**, 110 (1996).
[33]C. I. Wu and A. Kahn, Appl. Phys. Lett. **74**, 546 (1999).
[34]C. I. Wu, A. Kahn, E. S. Hellman, and D. N. E. Buchanan, Appl. Phys. Lett. **73**, 1346 (1998).
[35]C. D. Lee, Y. Dong, R. M. Feenstra, J. E. Northrup, and J. Neugebauer, Phys. Rev. B **68**, 205317 (2003).